

Pressure-induced structural phase transition and new superconducting phase in UTe_2

Fuminori Honda^{1,2,*}, Shintaro Kobayashi³, Naomi Kawamura³, Saori I. Kawaguchi³, Takatsugu Koizumi², Yoshiki J. Sato^{2,4}, Yoshiya Homma², Naoki Ishimatsu⁵, Jun Gouchi⁶, Yoshiya Uwatoko⁶, Hisatomo Harima⁷, Jacques Flouquet⁸, and Dai Aoki²

¹Central Institute of Radioisotope Science and Safety, Kyushu University, Fukuoka 819-0395, Japan

²Institute for Materials Research, Tohoku University, Oarai, Ibaraki 311-1313, Japan

³Japan Synchrotron Radiation Research Institute, Sayo, Hyogo 679-5198, Japan

⁴Department of Physics, Faculty of Science and Technology, Tokyo University of Science, Noda, Chiba 278-8510, Japan

⁵Faculty of Science, Hiroshima University, Higashi-Hiroshima, Hiroshima 739-8511, Japan

⁶Institute for Solid State Physics, University of Tokyo, Kashiwa, Chiba 277-8581, Japan

⁷Graduate School of Science, Kobe University, Kobe 657-8501, Japan

⁸Université Grenoble Alpes, CEA, Grenoble INP, IRIG, PHELIQS, F-38000 Grenoble, France

We report on the crystal structure and electronic properties under high pressure up to 11 GPa on a heavy fermion superconductor UTe_2 , as investigated by means of x-ray diffraction and electrical resistivity experiments. The x-ray diffraction measurements under high pressure using a synchrotron light source reveal anisotropic linear compressibility of the unit cell up to 3.5 GPa, while a pressure-induced structural phase transition is observed above $P_{\text{O-T}} \sim 3.5 - 4$ GPa at room temperature, where the body-centered orthorhombic crystal structure with the space group $Immm$ changes into a body-centered tetragonal structure with the space group $I4/mmm$. The molar volume drops abruptly at $P_{\text{O-T}}$, while the distance between the first-nearest neighbor of U atoms, $d_{\text{U-U}}$ abruptly increases, implying a switch from the heavy electronic states to the weakly correlated electronic states. Surprisingly, a new superconducting phase at high pressures above 7 GPa was detected at $T_{\text{sc}} > 2$ K with a relatively low upper-critical field, $H_{\text{c}2}(0)$. The resistivity above 3.5 GPa, thus in the high-pressure tetragonal phase, shows a large drop below 230 K, revealing a drastic change from the heavy electronic states to the weakly correlated state.

1. Introduction

UTe_2 is one of the hottest topics in condensed matter physics, because of its unusual superconducting properties, such as topological superconductivity, field-reentrant superconductivity, and multiple superconducting phases in a magnetic field as well as under high-pressure.¹⁻⁷⁾ A possible analogy to ferromagnetic superconductors, such as UGe_2 ,⁸⁾ URhGe ,⁹⁾ and UCoGe ¹⁰⁾ had been pointed out at the beginning of the discovery of superconductivity in UTe_2 .

Indeed, the huge field-reentrant superconductivity detected in the hard-magnetization axis in UCoGe ¹⁰⁾ and URhGe ⁹⁾ resembles that observed in UTe_2 for $H \parallel b$ -axis. On the other hand, no magnetic ordering was found down to low temperatures, revealing a paramagnetic ground state in UTe_2 ,¹¹⁾ which is quite in contrast to the above-mentioned ferromagnetic superconductors.

In UTe_2 , a first order metamagnetic transition is observed at $H_{\text{m}} \sim 35$ T at low temperature.^{1,12-15)} Although UTe_2 had been considered at the verge of the ferromagnetic ordering, no microscopic evidence for ferromagnetic interactions was obtained experimentally. On the other hand, inelastic neutron scattering experiments clearly detected the anti-ferromagnetic fluctuations at the incommensurate wave vec-

tor,^{16,17)} Recently, STM experiments lead to the observation of the charge density wave (CDW)¹⁸⁾ or the pair density wave (PDW)¹⁹⁾ in the superconducting state. After three years of studies, UTe_2 is found to be a remarkable heavy-fermion system, where the electronic, magnetic, and charge instabilities coupled to the occupancy of the $5f$ levels play important roles.²⁰⁾

To date, the relationship between the crystal structure and electronic properties is intensively discussed. Hence, we recall the crystal structure of UTe_2 . UTe_2 crystallizes in the body-centered orthorhombic structure with the space group $Immm$ (No. 71, D_{2h}^{21}),²¹⁾ where 4 formula units are included in the “conventional unit cell” ($Z = 4$). The nearest and next nearest neighbor U atoms locate along the c - and a -axes forming a rectangular shape within the ac -plane. It is also pointed out that the nearest U forms a two-leg ladder along the a -axis. The crystal structure is so-called UTe_2 -type, and few other materials form this structure, demonstrating that it is a quite unique structure. Note that further lowering symmetry from the space group $Immm$ in the electronic system is theoretically proposed,²²⁾ as it is known in the “hidden order” compound URu_2Si_2 .

The superconducting properties of UTe_2 depend strongly on its sample quality.^{20,23,24)} It is also claimed that significant deficiency of U rather than Te affects the elec-

*honda.fuminori.790@m.kyushu-u.ac.jp

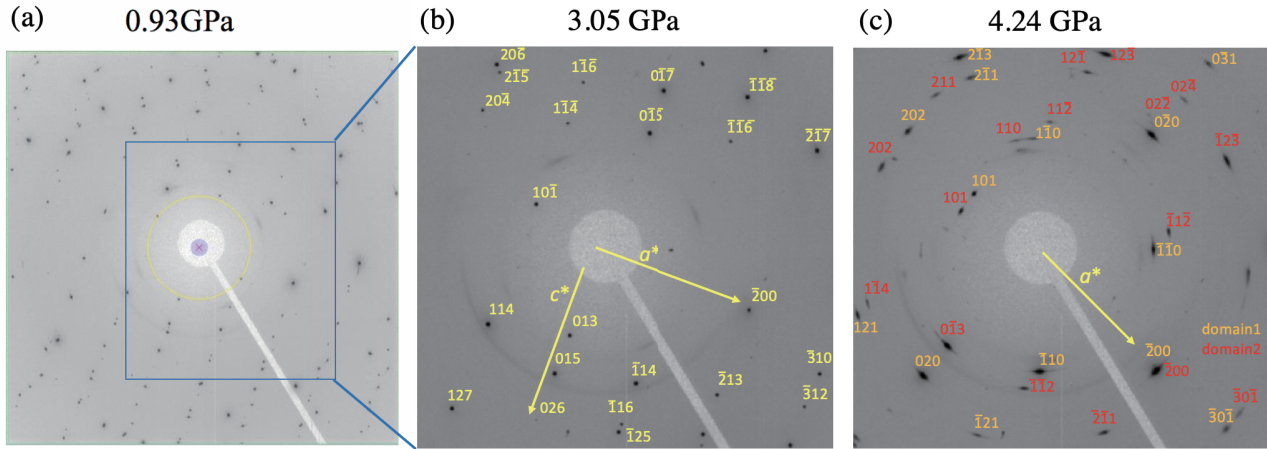


Fig. 1. (Color online) Single-crystal XRD patterns at (a) 0.93 GPa, (b) 3.05 GPa with the low-pressure orthorhombic phase, and (c) 4.24 GPa, with the high-pressure tetragonal phase measured at 300 K. The corresponding Miller indices are labeled in panels (b) and (c) on the basis of the orthorhombic and tetragonal structure, respectively. The crystal orientations in the reciprocal space are also shown by arrows. In panel (c), XRD patterns are indexed on the basis of two different domains, “domain 1” and “domain 2”

tronic/superconducting properties of UTe_2 from their precise analysis, indicating that there may be an instability in the crystal structure of UTe_2 .²⁵⁾

The pressure response of UTe_2 is very sensitive, displaying different superconducting and magnetic states. Applying the pressure, the superconducting transition temperature splits above 0.3 GPa, revealing multiple superconducting phases. At around 1 GPa, an unusual enhancement of H_{c2} for $H \parallel a$ -axis was detected at low temperature and high field region as a consequence of the multiple superconducting phases.^{26,27)} Even at ambient pressure, multiple superconducting phases were also detected for the b -axis in specific heat measurements associated with the field-reentrant superconducting state. Above the critical pressure of $P_c = 1.5$ GPa, superconductivity is suppressed and the magnetically ordered phase, most likely antiferromagnetism, appears under higher pressure.^{4,27)}

It is surprising that UTe_2 reveals such rich and unexpected phase diagrams under pressure and a magnetic field. This is most likely due to a singularity of the crystal structure and its instability. It is important to elucidate the pressure response of the crystallography and the electronic state at high pressures with good hydrostatic conditions using a high-quality single crystal. Here, we performed x-ray diffraction (XRD) experiments and resistivity up to 10 GPa. We found a drastic change in the crystal structure from the orthorhombic structure (space group: $Immm$) to the tetragonal structure ($I4/mmm$) above the critical pressure, $P_{O-T} \sim 3.5 - 4$ GPa at room temperature. Furthermore, the resistivity above 3.5 GPa shows a new phase transition around 230K, which is almost unchanged with increasing pressure up to 9 GPa. In addition, a reappearance of superconductivity was found at 9 GPa with low H_{c2} , indicating weak electronic correlations, in drastic contrast to superconductivity at low pressures. These results have been briefly

reported in JPS meeting and LT29 by oral and poster presentation, respectively.²⁸⁾

2. Experimental Procedure

Single crystals of UTe_2 were grown by the chemical vapor transport method using iodine as a transport agent as described in the ref. 2. The quality of single crystals was checked by the sharpness of the x-ray Laue pattern. The residual resistivity ratios at ambient pressure were 20–30, and a sharp specific heat jump due to the superconducting transition was detected at 1.6 K.

The XRD experiments under high pressure were carried out on the BL10XU beamline at the JASRI/SPring-8, Japan using a wavelength of $\lambda = 0.4130$ Å. Since UTe_2 is easily oxidized or damaged in particular for tiny pieces of samples, special attention was paid. Three XRD experiments using diamond anvil cells (DAC) were performed, where two of them were done on single crystals with different orientations, and the other was done with pulverized powder from the same batch of the single crystal. For the experiments using single crystals, two single crystals of UTe_2 , namely a crushed single crystal piece with having (010) plane with a size of $90 \mu\text{m} \times 90 \mu\text{m}$, and a thickness of $30 \mu\text{m}$ (labeled with “single (1st)”), and an oriented crystal with having (100) plane with a size of $120 \mu\text{m} \times 80 \mu\text{m}$, and a thickness of $23 \mu\text{m}$ by polishing (labeled with “single (2nd)”) were loaded in different DAC setups with SUS gaskets together with helium as pressure transmitting medium in order to get compensated diffraction data. XRD using a powder sample was also performed using helium as pressure transmitting medium. The pressure inside the DAC was measured using the conventional ruby scale both before and after the diffraction measurements. The sample pressure was regulated by a helium gas compression system. An imaging plate was used to obtain two-dimensional diffraction patterns via oscillation photography methods, and the resulting data were

integrated along the radial direction to get a 1-dimensional (1D) diffraction pattern.

Electrical resistivity under high pressures up to 9 GPa was measured by means of a conventional four-probe method with the current along the a -axis, using a Palm Cubic anvil press system²⁹⁾ installed at the Institute of Solid State Physics, the University of Tokyo in a ^4He cryostat down to 2 K. A mixture of Fluorinert FC70 and FC 77 with a 1:1 ratio was used as a pressure-transmitting medium. Good hydrostaticity of the pressure condition in this cubic anvil press was mainly guaranteed by the system itself, where the Teflon capsule inside the cubic pyrophyllite and/or MgO gasket was compressed from the 6 directions simultaneously. At 9 GPa, the lowest temperature was further extended down to 30 mK in a dilution refrigerator, and the magnetic field was applied along the c -axis of the original orthorhombic structure.

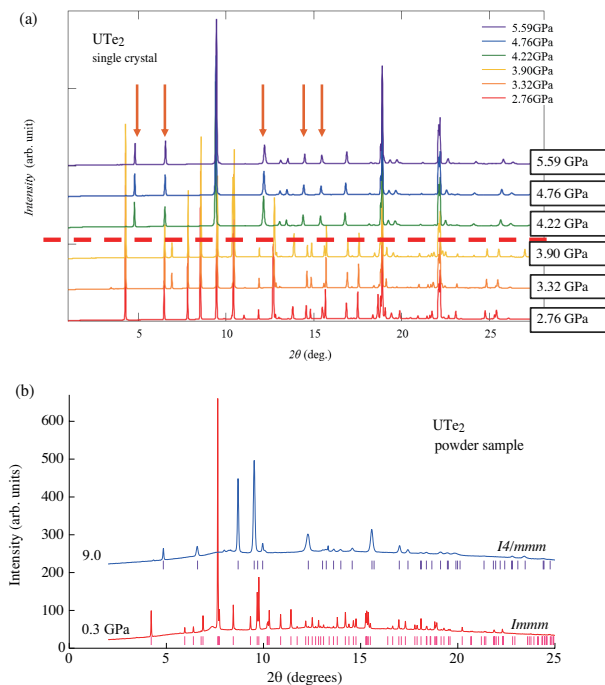


Fig. 2. (Color online) (a) XRD patterns of UTe_2 on a single crystal. The arrows at high pressure above 4 GPa indicate the characteristic peaks of the high-pressure tetragonal phase. (b) XRD patterns on powder samples at 0.3 and 9.0 GPa, where vertical lines in red and blue are calculated peak positions based on orthorhombic ($Immm$) and tetragonal ($I4/mmm$) structures, respectively.

3. Experimental Results and Analyses

3.1 x-ray diffraction under high pressure

Figure 1 shows the XRD patterns of a crushed UTe_2 single crystal (“single (1st)”) at (a) 0.93, (b) 3.05, and (c) 4.24 GPa at room temperature. To obtain more diffraction spots, the pressure cell was swung by ± 10 degrees around the origin. Here, Figs. 1(b) and 1(c) are focused on magnifying in the

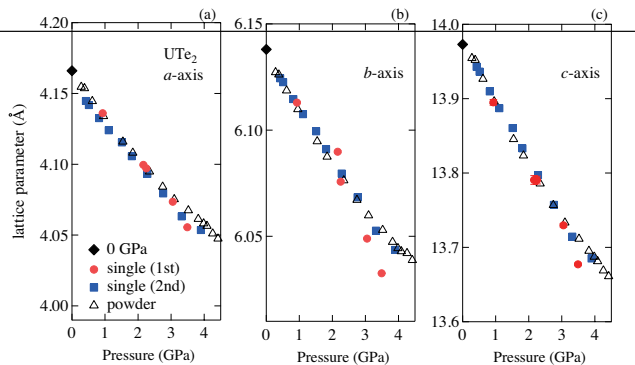


Fig. 3. (Color online) Pressure dependences of lattice parameters for orthorhombic structures at low pressures. Open and closed symbols indicate the results obtained from single crystals and powder samples, respectively. Data at ambient pressure are taken from Ref.21.

rectangular area of Fig. 1(a) for clarity. The diffraction patterns at 0.93 and 3.05 GPa are well reproduced by the diffraction patterns of the reported orthorhombic structure with the space group $Immm$. The Miller indices of each diffraction spot are indicated on the basis of that structure in Fig. 1(b). Directions of the approximate reciprocal vectors are also indicated by arrows. On the other hand, it is easily recognized that the diffraction pattern at 4.24 GPa has changed drastically. It should be noted that the diffraction pattern changed during the measurement at 3.49 GPa, thus the structural phase transition occurs at this pressure on “single (1st)” sample. Upon compression of the sample above 3.5 GPa, the number of Bragg peaks is almost doubled. This indicates that the sample transformed to multi-domain and/or the lattice symmetry becomes lowered. Those observed Laue spots are obviously broadened and start to form so-called Debye–Scherrer rings (change their shapes ellipsoidal). The Miller indices of each diffraction spot in Fig. 1(c) are indicated on the basis of the tetragonal structure with the space group $I4/mmm$ including two domains, which is explained in more detail later.

The obtained 2-dimensional (2D) diffraction patterns are converted into 1D intensity 2θ angle profiles by integrating along the radial direction from the beam center in order to analyze unit cell parameters. Figure 2(a) shows diffraction peaks of UTe_2 obtained from a single crystal with the (110) plane (“single (2nd)”) under high pressures at room temperature. Since the patterns are obtained from a single crystal (single domain), not all the diffracted peaks expected from the orthorhombic crystal structure with the space group $Immm$ were observed and the relative height of the peak intensities was not well reproduced, but they were sufficient to determine lattice parameters. It is again clear that the diffraction patterns have changed after 4 GPa. Above 4 GPa, the observed XRD pattern was indexed to a body-centered tetragonal system to give the following crystal structure parameters: $a = 3.89 \text{ \AA}$ and $c = 9.80 \text{ \AA}$. The detailed crystal structure analysis of the high-pressure tetragonal phase is described in the following section. The a -axis and c -axis direction in the low-pressure phase turns to nearly a -axis through the structural phase transition,

which means the original a -axis in the orthorhombic structure almost keeps its orientation in the high-pressure tetragonal phase. In order to confirm the structural change from $Immm$ to $I4/mmm$, the XRD using powder samples were displayed at 0.3 and 9.0 GPa as shown in Fig. 2(b). The diffraction patterns at 0.3 and 9.0 GPa were well explained by the calculated peak positions with the lattice parameters of the low-pressure orthorhombic ($Immm$) with $a = 4.155$, $b = 6.127$, and $c = 13.954$ Å, and high-pressure tetragonal ($I4/mmm$) phases with $a = 3.859$ and $c = 9.775$ Å, respectively. The pressure-induced tetragonal structure was found to be retained at least up to 11 GPa, the highest pressure measured in this study.

From these results, we determined the pressure dependence of the lattice parameters of UTe_2 both from single crystals and from powder samples. The analyzed unit cell parameters of the orthorhombic a -, b -, and c -axes as a function of pressure are shown in Figs. 3(a), 3(b), and 3(c), respectively. The results from single crystals and powder samples are basically the same. Lattice parameters along a -, b -, and c -axes decrease almost linearly with increasing pressure. The compression curves are anisotropic and the obtained linear compressibility ($k_i = -(1/L_i)dL_i/dp)_{p=0}$, $i = a, b, c$ -axes), where L_i is a lattice parameter along the crystallographic i -axis, is $k_a = 7.2 \times 10^{-3}$, $k_b = 4.0 \times 10^{-3}$, and $k_c = 5.8 \times 10^{-3}$ (GPa^{-1}) for a -, b -, and c -axes, respectively. The a -axis is the most compressive and the b -axis is the hardest. The elastic properties of uranium compounds are not well established, so far, due to a lack of sufficient examples. However, it is suggested empirically that the direction of U-U bonds is distinctly the “soft” crystallographic direction in UTX (T: transition metal, X: metalloid) system, since the $5f$ -electrons of U participate in the bonding.^{30,31} In UTe_2 , the direction along the c - and a -axes corresponds to the 1st and 2nd nearest neighbor U-bonding, respectively, and shows larger linear compressibility compared to that along the b -axis, which is consistent with the above-mentioned hypothesis. The calculated volume compressibility $k_V = k_a + k_b + k_c = 17 \times 10^{-3}$ (GPa^{-1}) corresponds to the bulk modulus of $B = 59$ GPa. This value is even smaller than that of the tellurium element itself $B = 65$ GPa. UTe_2 is very “soft”. Thus, drastic changes in the physical properties in UTe_2 under pressure are caused by such small bulk modulus.

Figure 4 shows the molar volume change as a function of pressure up to 11 GPa at room temperature in single crystals (closed symbol) and powder (open symbol) samples. Pressure dependence of the relative volume change ($\Delta V/V_0 = (V(P) - V_0)/V_0$) with respect to the volume at ambient pressure (V_0) reaches already 3.5 % at 2 GPa, which is comparable to the volume reduction in liquid ^3He (about 5 %), where the paramagnetic Fermi liquid phase changes to the solid phase on the melting curve at low temperature. Thus, one can easily imagine the rather drastic change that occurs in the electronic properties of UTe_2 such as the disappearance of the superconductivity and an occurrence of the magnetic ordering under about 2 GPa.

The volume compression is analyzed by following Mur-

naghan equation of state,

$$\frac{V}{V_0} = \left[P \left(\frac{B'_0}{B_0} \right) + 1 \right]^{-1/B'_0}, \quad (1)$$

where B_0 and B'_0 are the bulk modulus and its pressure derivative at ambient pressure, respectively, and V_0 was calculated from the extrapolated lattice parameters to 0 GPa from the present pressure data. The best-fit parameters are $B_0 = 59$ GPa and $B'_0 = 1.9$. The dotted blue line in Fig. 4 is the calculated curve using these parameters and eq. 1. The molar volume drops at the structural phase transition with a volume change of 10 %. It should be noted that the crystal structure turned back to the original orthorhombic structure below 1 GPa during decreasing pressure, which indicates the latent heat at the structural transition is large.

The results between single crystal (closed symbol) and powder samples (open symbol) are basically similar, but the main difference is the critical pressure of structural transition and coexistence region of low- and high-pressure phases. The single crystal data show the transition to the tetragonal structure almost suddenly at $P_{O-T} = 3.5$ and 4 GPa, while the coexistence of two structures occurs between 5 and 7 GPa in powder sample. This is most likely due to the pressure distribution in the gasket and internal strain and/or defects that could happen in the pulverization of single crystals.

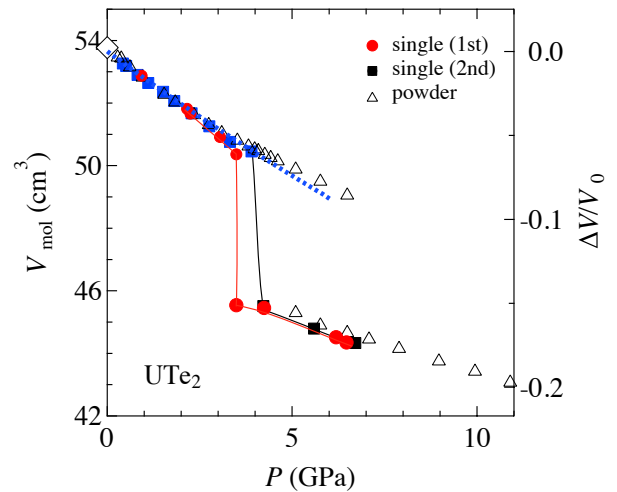


Fig. 4. (Color online) Pressure dependence of the molar volume in UTe_2 based on the orthorhombic ($Immm$) and tetragonal ($I4/mmm$) structure at 300 K. Closed and open symbols are the results from single crystals and powder samples, respectively. An open diamond is taken from Ref. 21. The right axis corresponds to the scaled volume change. The dotted blue line indicates the results of fitting by the Murnaghan equation of state. The solid red and black lines are guides for eyes.

3.2 Electrical resistivity under high pressure

Figure 5(a) shows the temperature dependence of the electrical resistivity $\rho(T)$ of UTe_2 single crystal with the current

along the orthorhombic a -axis at different pressures. The $\rho(T)$ curve in UTe_2 at ambient pressure is characterized by almost temperature independent above 100 K and an abrupt decrease of ρ below 50 K, as shown in the dashed line in Fig. 5(a). It should be noted that the bare LDA band structure calculation predicts a Kondo semiconductor in spite of the fact that the relatively large volume of Fermi surfaces (about 20 % in BZ for each hole and electron Fermi surface with the compensation) are experimentally detected.³²⁾ The Coulomb repulsion U and the strong correlation must be taken into account in the calculations³³⁾ in order to explain real Fermi surfaces, suggesting that the electronic states are sensitive to pressure and temperature. At 2 GPa, $\rho(T)$ still resembles the curve at ambient pressure with a gradually enhanced hump around 25 K, indicating that the heavy electronic state is still preserved or even enhanced at low temperatures. At lower temperatures, two anomalies are detected at 8.5 and 2.8 K, which may correspond to the transitions for the pressure-induced WMO and MO phases, respectively.²⁷⁾ At 3.5 GPa, $\rho(T)$ behavior changes drastically, where the electrical resistivity decreases monotonically with decreasing temperature and shows a clear shoulder around $T^{**} = 230\text{K}$ and a small upturn at around $T_m = 4\text{ K}$. The anomaly at T_m is consistent with the pressure-induced magnetic transition reported previously.^{4,5,27)} With increasing pressure above 5 GPa, the T_m anomaly smeared out, and T^{**} slightly increases monotonically with an initial slope of 1.9 K/GPa as shown in Fig. 5(b). The origin of the anomaly at T^{**} is not clear so far, but one can speculate that it corresponds to a drastic change from single site behavior to a well-coupled array at rather high temperatures, which is basically one order magnitude higher than the crossover temperature T^* detected at low pressure. Note that the value of resistivity at room temperature as a function of pressure shows no drastic change at the critical pressure $P_{\text{O-T}}$ for structural transition.

In order to investigate the low-temperature properties in more detail, resistivity experiments were extended at very low temperatures down to 30 mK. Figure 6(a) shows the low-temperature part of $\rho(T)$ under high pressure above 3.5 GPa of the high-pressure tetragonal phase. The onset of the pressure-induced superconductivity is detected at 7 GPa below 2 K. At 9 GPa, a clear superconducting transition by zero resistivity was detected below about 1 K. The onset of the superconducting transition temperature T_{SC} is 2.2 K at 9 GPa in a zero magnetic field, where the superconducting transition temperature is defined with 80 % of the residual resistivity. It should be noted that the broadened SC transition can be attributed to the strain and cracks arising due to the structural transition associated with the drastic change of lattice parameters. In fact, the sample unloaded from the Palm Cubic anvil pressure cell after the measurement breaks up into small pieces, which was also seen in the samples taken after the XRD measurements under pressure.

We further investigated the superconducting property at 9 GPa in magnetic field and constructed the phase diagram. Here, the magnetic field was applied along the original c -

axis in the low-pressure orthorhombic phase. Figures 6(b) and 6(c) show the temperature dependence of the electrical resistivity at the different magnetic fields and magnetic field dependence at 30 mK, respectively. Pressure-induced superconductivity disappears above 2.5 T, although the small onset of superconductivity persists up to about 3.8 T. We show in Fig. 6(d) the temperature dependence of the upper critical field H_{c2} defined as 80 % of the resistivity of the normal state. The slope of the upper critical field is $-dH_{c2}/dT \sim 1\text{ T/K}$ at $T_{\text{SC}} = 2.2\text{ K}$, and the value of $H_{c2}(T=0)$ is about 2.5 T, which is smaller than the Pauli limit based on the weak coupling BCS theory. Furthermore, the temperature dependence of the electrical resistivity follows the Fermi liquid behavior ($\rho = \rho_0 + AT^2$) with the small A coefficient ($A_{9\text{GPa}} \sim 1.4 \times 10^{-3} \mu\Omega \cdot \text{cm/K}^2$), indicating superconductivity is based on the weakly correlated electronic states without contribution from the $5f$ -electrons. This can be compared with the A coefficient at ambient pressure, $A_0 \sim 0.9 \mu\Omega \cdot \text{cm/K}^2$.²⁾ The ratio, $A_{9\text{GPa}}/A_0 \sim 600$ is comparable or the same order with $(T^{**}/T^*)^2 \sim 300$. Furthermore, the Sommerfeld coefficient for the specific heat is expected to be less than $10\text{ mJ K}^{-2}\text{mol}^{-1}$ at high pressure, assuming the Kadowaki-Woods ratio, suggesting a weak electronic correlation. The small initial slope of H_{c2} at 9 GPa is also reasonable, compared to the large values, 34 T/K and 7.5 T/K for b and c -axis, respectively, detected at ambient pressure, in accordance with the change of the effective masses, since H_{c2} is proportional to the $(m^*T_{\text{sc}})^2$ assuming the Fermi surfaces are unchanged.

It is known that conventional superconductivity of the tellurium element is induced above 4 GPa, but the superconducting state of tellurium is easily killed at the magnetic field of 0.03 T. Thus, the observed pressure-induced superconductivity is not due to the remaining tellurium but is intrinsic in the high-pressure tetragonal phase of UTe_2 .

Figure 7 shows the pressure-temperature phase diagram of UTe_2 . The structural transition from orthorhombic to tetragonal occurs at $P_{\text{O-T}} \sim 3.5 - 4\text{ GPa}$ at room temperature, and $P_{\text{O-T}}$ shifts to the higher pressure, $P_{\text{O-T}} \sim 5.5\text{ GPa}$ at 30 and 50 K.³⁴⁾ At low pressure above 1.5 GPa, T_{MO} corresponding to a magnetic order increases rapidly with pressure, and it disappears above 3.5 GPa. New anomalies denoted by T^{**} start appearing above 3 GPa, and are almost unchanged up to 9 GPa. Superconductivity reappears around 2 K in the tetragonal phase, where the electronic state is drastically changed without the strong electronic correlations as demonstrated by resistivity curves and the low H_{c2} .

4. Discussion

4.1 Pressure-induced structure transition at high pressure

We discuss the pressure-induced structural transition around $P_{\text{O-T}} \sim 3.5-4\text{ GPa}$. The observed diffraction patterns above $P_{\text{O-T}}$ are quite different from the ones in the orthorhombic phase. The diffraction pattern is found to be reproduced with two domains of the body-centered tetragonal (BCT) lattice with $a \sim 3.98\text{ \AA}$ and $c \sim 9.80\text{ \AA}$, taking into account the extinction rule.

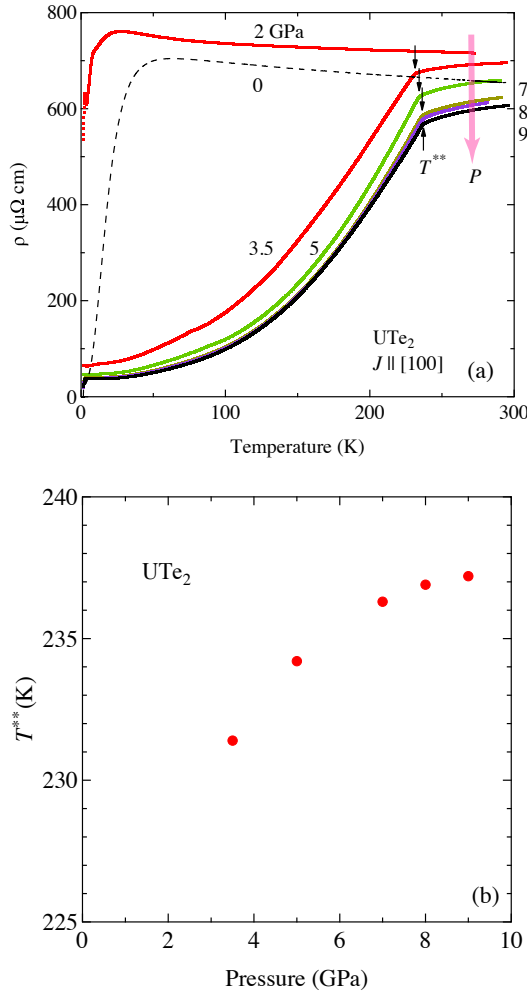


Fig. 5. (Color online) (a) Resistivity at different pressures up to 9 GPa for $J \parallel a$ -axis in UTe_2 . The data at ambient pressure shown by the dotted line are taken from Ref. 2. (b) Pressure dependence of T^{**} .

The volume of the conventional unit cell at ambient pressure is 357 \AA^3 with $Z = 4$, whereas, above P_{O-T} , that of the tetragonal lattice is about 149 \AA^3 . This corresponds to $Z \sim 2$ realized in the high-pressure tetragonal structure and is consistent with the BCT lattice. Thus, the possible space groups of the high-pressure structure are $I4/mmm$ or its subgroups. Here, we simply take $I4/mmm$ as it's the symmetry of the lattice. It is natural to assume that U atoms are located at the lattice points, namely at the site $2a$ (0 0 0). Given that the Te atoms occupy a crystallographically equivalent site, the position would be limited to site $4c$ (0 1/2 0), $4d$ (1/2 0 1/4) or $4e$ (0 0 z). Among them, the U-Te distance is 1.99 \AA for Te at the $4c$ site and the Te-Te distance is 2.81 \AA for Te at the $4d$ site, which seems too short considering the ionic radius and strong Coulombic interaction, respectively. While, the Te in the $4e$ site, with $z \sim 1/3$, gives the U-Te and Te-Te distances of about 3.2 \AA , which appears to be more reasonable than in the other cases above. The simulated XRD pattern assuming

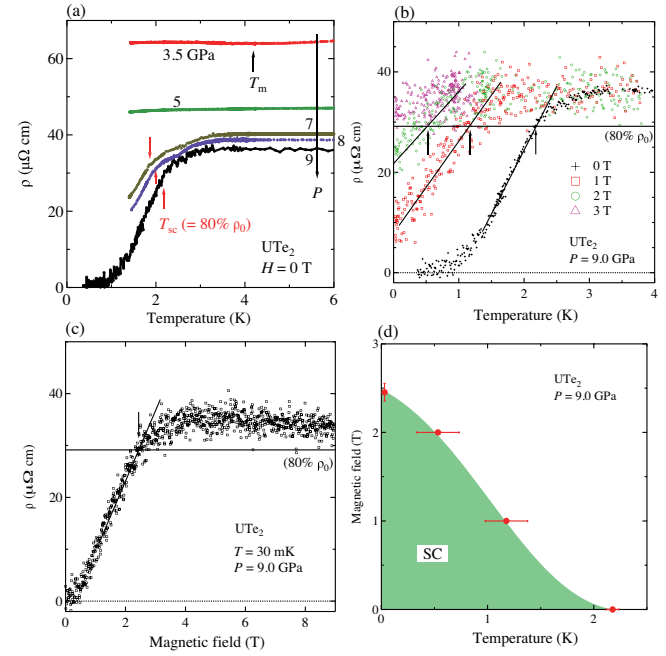


Fig. 6. (Color online) (a) Low-temperature resistivities at different pressures above 3.5 GPa in UTe_2 . (b) Low-temperature resistivities at different fields at 9 GPa. (c) Field dependence of the resistivity at the lowest temperature, 30 mK at 9 GPa. (d) Superconducting phase diagram at 9 GPa. Here T_{sc} or H_{c2} are defined by the temperature or field, at which the resistivity is reduced to the value of 80% from the normal state resistivity.

this structure reproduces well the powder XRD pattern of the high-pressure phase as shown in Fig. 2(b). The crystal structure of the low-pressure (LP) orthorhombic and high-pressure (HP) tetragonal phases are depicted in Figs. 8(a) and 8(c), respectively. It should be noted that the structural phase transition from the ambient-pressure $Immm$ phase of UTe_2 into a ten-fold coordinated, where Te is at $4e$ site, high-pressure $I4/mmm$ phase at 9 GPa is suggested by theoretical calculations.³⁸⁾

For these drastic changes in the crystal structure and lattice parameters, large atomic displacements are inevitably required. Three possible unit cells that could be transformed into the body-centered tetragonal structure are shown in Figs. 8(d)-8(f). In all cases, the ab -plane for the tetragonal structure is based on the close distances for the 1st and 2nd nearest neighbors, $d_1 \sim 3.78 \text{ \AA}$ and $d_2 \sim 4.17 \text{ \AA}$, respectively. In Fig. 8(d), the rung denoted by d_1 should be tilted, moreover, the atomic position must move to the a -axis in order to get the tetragonal structure. The direction for the new c -axis in the tetragonal structure approximately corresponds to the reciprocal $[011]$ direction in the orthorhombic structure. Note that the reciprocal $[011]$ direction (24 deg tilted from b to c -axis) is different from $[011]$ direction in real space (24 deg tilted from c to b -axis). In Fig. 8(e), the rung should be also tilted, but no atomic displacement is required along a -axis. The new c -axis approximately corresponds to the $[011]$ direction in real space. In Fig. 8(f), a U atom largely moves

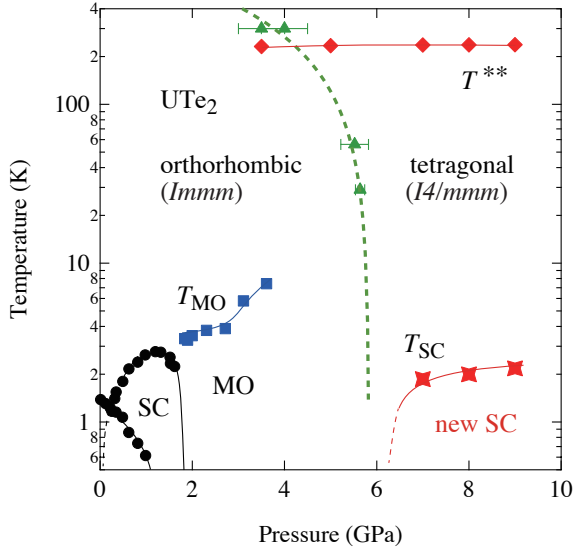


Fig. 7. (Color online) Pressure-temperature phase diagram of UTe_2 up to 10 GPa. Solid lines are guides to the eyes. Solid triangles correspond to the structural phase transition from orthorhombic to tetragonal structure detected at different temperatures. The data points for low-pressure superconductivity (SC) are taken from Ref.4. The dotted green line is the linear extrapolation of P_{O-T} .

along the orthorhombic c -axis to get the body-centered tetragonal structure. This is rather simple displacement of U atoms, indicating that the orthorhombic b -axis switches to the tetragonal c -axis.

Although we cannot determine which atomic displacement is correct, we speculate that the $[011]$ or the reciprocal $[011]$ directions is important and it is related to the structural instabilities. Compared with the crystal structures in LP and HP phases focusing on the U position, the rectangular arrangement of U atoms in the ac -plane in the LP phase seems to correspond to the basal plane in the HP tetragonal phase. In this structure transformation, the crystal along the a -axis keeps its direction, and the ac -plane including the U rectangular tilts about 25 degrees from the b to c -axis. With this transformation, the $[011]$ direction in the reciprocal space in the LP orthorhombic phase, most likely, turns to the $[001]$ axis in the HP tetragonal axis. It means that the reciprocal $[011]$ direction in the LP phase has been already potentially important in the stability of the crystal structure. It should be noted that the above-mentioned transformation is consistent with the change of the Laue spots as shown in Fig. 1(b) into 1(c).

Since our experiments were carried out on single crystals, not all the diffraction peaks from the tetragonal structure can be obtained. It brings difficult to determine the atomic position of Te precisely. It is known that several proto-type compounds crystallize in the tetragonal $I4/mmm$ type, with AB_2 composition. For example, MoSi_2 , WSi_2 and WGe_2 are typical compounds, where the c/a ratio is quite similar to the pressure-induced HP phase in UTe_2 and z parameters are 0.335 in these cases.³⁵⁻³⁷ From the theoretical calculation, Hu

et al. predict $z = 0.337$.³⁸ Here, we assume the z parameter to be 0.335 in the HP phase in UTe_2 based on the z parameter of the proto-type compounds, which is close to the theoretical prediction. The pressure dependence of the 1st and 2nd nearest neighbor U distances are depicted Fig. 9. The diverse interatomic distances become more simply in the high-symmetry structure of the $I4/mmm$ tetragonal phase. Note that UTeAs , UTeP , and UTeGe are known to form the tetragonal structure with the space group $I4/mmm$. The c/a ratio is, however, much larger, and 4 molecules exist in the unit cell ($Z = 4$).

It is worth mentioning that the c -axis in the high-pressure phase corresponds to the reciprocal $[011]$ direction in the original low-pressure structure, which is tilted by 24 deg from the b to c -axis. Huge field-reentrant superconductivity is observed around this field direction above the metamagnetic field $H_m \sim 40\text{--}50$ T. According to the band calculation of $\text{GGG}+U$ ($U = 2$ eV) based on the $5f$ -itinerant model, the maximal and minimal cross-sectional areas of the electron Fermi surface coincide for the field direction to the reciprocal $[011]$ direction, which is the so-called Yamaji angle. The increase of the density of states is generally expected under a magnetic field at Yamaji angle, and indeed in UTe_2 , the specific heat increases with the field, showing a positive jump at H_m .¹⁵ Furthermore the drastic change of Hall resistivity is also found for the field direction along b -axis and the reciprocal $[011]$ direction.^{39,40}

This suggests that Fermi surface instabilities play a role in field-reentrant superconductivity around $[011]$ direction above H_m . The switching principal axis to the original reciprocal $[011]$ direction can be another mark of these Fermi surface instabilities. One can thus expect further singularities along the $[011]$ or the reciprocal $[011]$ direction by uniaxial stress, thermal expansion and ultrasound experiments.

It is interesting that the flat crystal surface perpendicular to the reciprocal $[011]$ as well as $[001]$ direction appear often on as-grown single crystals by the chemical transport method and by the flux method. The natural crystal surface is generally related to the growth speed, which could be affected by the crystal structure. This may indicate a precursor for the singularity of the reciprocal $[011]$ direction.

4.2 Pressure-induced electronic phase transitions

Two pressure-induced phase transitions appear in UTe_2 for its electronic states in the high-pressure tetragonal phase. One is characterized by the kink of the electrical resistivity at $T^{**} = 230$ K and the other one is a superconducting phase transition around 2 K. The former transition was also observed in the previous study.⁴¹ In their report, the T^{**} anomaly was observed for the geometry $H \parallel b$ which makes internal strain along the b -axis ($u \parallel b$), with their semi-hydrostatic Bridgman anvil cell, but no anomaly was observed for the geometry $H \parallel c$ ($u \parallel c$), suggesting that the T^{**} anomaly is sensitive to the uniaxial stress. The hydrostaticity of the pressure in our Palm Cubic anvil-type pressure cell is guaranteed by the design itself independent of the pressure-transmitting medium. Therefore, The T^{**} anomaly can be fa-

avorable to the compression along the b -axis in the LP phase. When the unit cell is compressed along the b -axis, the atomic displacement occurs to avoid strong Coulomb repulsion, particularly between Te(2) sites mentioned above. It is known that several uranium pnictides and chalcogenides exhibit high magnetic ordering temperatures.⁴³⁾ Thus, it is not surprising that the magnetic order could occur at high-temperature in UTe_2 . The nearest neighbor uranium distance in the high-pressure phase of UTe_2 reaches 3.9 Å which is sufficiently larger than the so-called Hill limit. Therefore it could be possible that the T^{**} anomaly is attributed to a switch from $5f$ single site behavior to coupled $5f$ array. The nature of the transition is the primary task for future study. The resistivity anomaly is resembling a conventional 2nd-order phase transition in a ferromagnet (or antiferromagnet without a superzone boundary effect - possible for the suggested structure assuming an AF coupling within one unit cell with magnetic propagation vector $k = (0\ 0\ 0)$). However, without further study, we cannot exclude other options such as a valence change or a kind of Lifshitz transition at the pressure-driven transition.

It is clear that the observed superconductivity at high pressure cannot be attributed to the heavy electronic state, as shown by low $H_{c2}(0)$ and small A coefficient. The drastic change of electronic states associated with the structural change may invoke a new superconducting state without $5f$ -electron correlation. A key point is that the distance between the nearest neighbors of U atoms suddenly increases at the critical pressure from orthorhombic to tetragonal structure as shown in Fig. 9, despite the fact that volume decreases with pressure; this leads to the non-trivial results of $5f$ occupancy, which jumps to 4 % higher than that at ambient pressure.

Similar conclusions were recently given on the pressure studies,⁴²⁾ where the transition from the orthorhombic to tetragonal transition is reported at around 5 GPa under the quasi-hydrostatic condition, associated with an increase of the Bulk modulus by 45 % which reaches a value above the critical pressure of the structural transition. This is close to a full valence state and the spectacular boost of d_{U-U} by 8 %. The value of d_{U-U} is even larger than that at ambient pressure. Furthermore, a new key result is that a trivalent state of U atom recovers at high pressure in the tetragonal structure.⁴⁴⁾

Qualitatively these observations are in agreement with the theoretical calculations,³⁸⁾ in which a structural transition from orthorhombic to tetragonal is predicted at 9 GPa; the main pressure effect is to boost the chemical bonding of the pair of Te electrons. A large Bulk modulus is also predicted just above the critical pressure. Quantitative differences critical parameters between experiments and theory is most likely the difficulty of the treatment for the strong correlation effect in UTe_2 .

5. Summary

We have performed the XRD experiments using single crystals and powder samples to clarify the pressure effect of the crystal structure as well as the electrical resistivity measurements under high pressure up to 9 GPa. X-ray diffrac-

tion study under high pressure reveals anisotropic linear compressibility of the unit cell, up to 3 GPa, and a pressure-induced structural phase transition above around 3.5 - 4 GPa at room temperature. The body-centered orthorhombic crystal structure with the space group $Immm$ transforms into a body-centered tetragonal structure with the space group $I4/mmm$. In addition, we have observed a drastic change in the electronic states accompanied by the structural phase transition and the reappearance of superconductivity above 7 GPa, which does not correspond to heavy fermion superconductivity. This could be linked to a quite rare case, where the U^{3+} configuration is recovered at high pressure.⁴⁴⁾

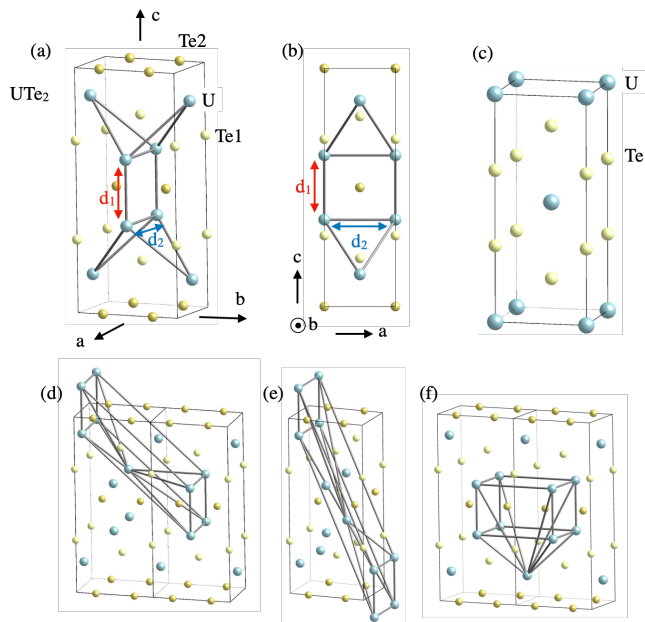


Fig. 8. (Color online) (a) Orthorhombic structure with the space group $Immm$ at low pressure. (b) A view from b -axis. The distances of the 1st and 2nd nearest neighbors of U atoms are $d_1 = 3.78$ Å and $d_2 = 4.17$ Å, respectively. (c) Tetragonal structure with the space group $I4/mmm$ at high pressure. (d)(e)(f) Three possible unit cells for the transformation to the body-centered tetragonal structure are displayed by bonds between U atoms.

Acknowledgement

The authors would like to thank W. Knafo, L. Havela, F. Wilhelm, and J. P. Sanchez for the fruitful discussion, and S. Nagasaki for the technical support. This work was performed with the approval of the Japan Synchrotron Radiation Research Institute (JASRI) (Proposal Nos. 2020A0741, 2020A0740, and 2021A1527) and under the Inter-University Cooperative Research Program of the Institute for Materials Research, Research Center for Nuclear Materials Science of Tohoku University (Proposal Nos. 202012-IRKAC-0017, 202012-IRKAC-0056, 202112-IRKAC-0029, and 202112-IRKAC-0041). This work was financially supported by KAKENHI

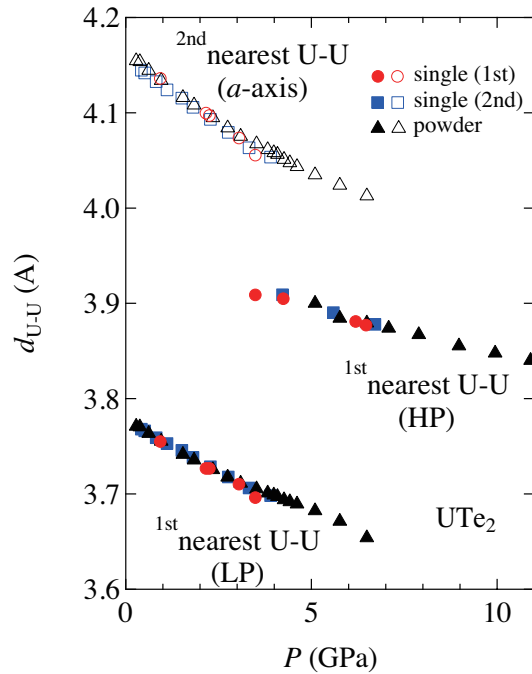


Fig. 9. (Color online) Pressure dependence of the distance of the 1st nearest neighbor of U atoms, d_1 (closed symbols). The 2nd nearest neighbor, d_2 at low pressure is also shown (open symbols). The results of single crystals, 1st run, 2nd run and powder sample are shown by circles, square, and triangle, respectively.

(JP19K21840, JP19H00648, JP20K03827, JP20K20889, JP20H00130, JP20KK0061, JP22H04933, JP22K03516).

- 1) S. Ran, C. Eckberg, Q.-P. Ding, Y. Furukawa, T. Metz, S. R. Saha, I.-L. Liu, M. Zic, H. Kim, J. Paglione, and N. P. Butch, *Science* **365**, 684 (2019).
- 2) D. Aoki, A. Nakamura, F. Honda, D. Li, Y. Homma, Y. Shimizu, Y. J. Sato, G. Knebel, J.-P. Brison, A. Pourret, D. Braithwaite, G. Lapertot, Q. Niu, M. Vališka, H. Harima, and J. Flouquet, *J. Phys. Soc. Jpn.* **88**, 043702 (2019).
- 3) G. Knebel, W. Knafo, A. Pourret, Q. Niu, M. Vališka, D. Braithwaite, G. Lapertot, J.-P. Brison, S. Mishra, I. Sheikin, G. Seyfarth, D. Aoki, and J. Flouquet, *J. Phys. Soc. Jpn.* **88**, 063707 (2019).
- 4) D. Braithwaite, M. Vališka, G. Knebel, G. Lapertot, J. P. Brison, A. Pourret, M. E. Zhitomirsky, J. Flouquet, F. Honda, and D. Aoki, *Commun. Phys.* **2**, 147 (2019).
- 5) D. Aoki, F. Honda, G. Knebel, D. Braithwaite, A. Nakamura, D. Li, Y. Homma, Y. Shimizu, Y. J. Sato, J.-P. Brison, and J. Flouquet, *J. Phys. Soc. Jpn.* **89**, 053705 (2020).
- 6) S. Ran, H. Kim, I.-L. Liu, S. Saha, I. Hayes, T. Metz, Y. S. Eo, J. Paglione, and N. P. Butch, *Phys. Rev. B* **101**, 140503R (2020).
- 7) S. Ran, I.-L. Liu, Y. S. Eo, D. J. Campbell, P. Neves, W. T. Fuhrman, S. R. Saha, C. Eckberg, H. Kim, J. Paglione, D. Graf, J. Singleton, and N. P. Butch, *Nat. Phys.* **15**, 1250 (2019).
- 8) S. S. Saxena, P. Agarwal, K. Ahilan, F. M. Grosche, R. K. W. 26) Haselwimmer, M. J. Steiner, E. Pugh, I. R. Walker, S. R. Julian, P. Monthoux, G. G. Lonzarich, A. Huxley, I. Sheikin, D. Braithwaite, and J. Flouquet, *Nature* **406**, 587 (2000).
- 9) D. Aoki, A. Huxley, E. Ressouche, D. Braithwaite, J. Flouquet, J.-P. Bri-

- son, E. Lhotel, and C. Paulsen, *Nature* **413**, 613 (2001).
- 10) N. T. Huy, A. Gasparini, D. E. de Nijs, Y. Huang, J. C. P. Klaasse, T. Gortenmulder, A. de Visser, A. Hamann, T. Görlach, and H. v. Löhneysen, *Phys. Rev. Lett.* **99**, 067006 (2007).
- 11) S. Sundar, S. Gheidi, K. Akintola, A. M. Côté, S. R. Dunsiger, S. Ran, N. P. Butch, S. R. Saha, J. Paglione, and J. E. Sonier, *Phys. Rev. B* **100**, 26) 140502(R) (2019).
- 12) A. Miyake, Y. Shimizu, Y. J. Sato, D. X. Li, A. Nakamura, Y. Homma, F. Honda, J. Flouquet, M. Tokunaga, and D. Aoki, *J. Phys. Soc. Jpn.* **88**, 063706 (2019).
- 13) W. Knafo, M. Vališka, D. Braithwaite, G. Lapertot, G. Knebel, A. Pourret, J.-P. Brison, J. Flouquet, and D. Aoki, *J. Phys. Soc. Jpn.* **88**, 063705 (2019).
- 14) G. Knebel, M. Vališka, M. Kimata, F. Honda, D. Li, D. Braithwaite, G. Lapertot, W. Knafo, A. Pourret, J.-P. Brison, J. Flouquet, and D. Aoki, *J. Phys. Soc. Jpn.* **89**, 053707 (2020).
- 15) A. Miyake, Y. Shimizu, Y. J. Sato, D. X. Li, A. Nakamura, Y. Homma, F. Honda, J. Flouquet, M. Tokunaga, and D. Aoki, *J. Phys. Soc. Jpn.* **90**, 103702 (2021).
- 16) C. Duan, K. Sasmal, M. B. Maple, A. Podlesnyak, J.-X. Zhu, Q. Si, and P. Dai, *Phys. Rev. Lett.* **25**, 237003 (2020).
- 17) W. Knafo, G. Knebel, P. Steffens, K. Kaneko, A. Rosuel, J. P. Brison, J. Flouquet, D. Aoki, G. Lapertot, and S. Raymond, *Phys. Rev. B* **104**, L100409 (2021).
- 18) A. Aishwarya, J. May-Mann, A. Raghavan, L. Nie, M. Romanelli, S. Ran, S. R. Saha, J. Paglione, N. P. Butch, E. Fradkin, and V. Madhavan, arXiv:2207.09491.
- 19) Q. Gu, J. P. Carroll, S. Wang, S. Ran, C. Broyles, H. Siddiquee, N. P. Butch, S. R. Saha, J. Paglione, J. S. Davis, and X. Liu, arXiv:2209.10859.
- 20) D. Aoki, J. P. Brison, J. Flouquet, K. Ishida, G. Knebel, Y. Tokunaga, and Y. Yanase, *J. Phys.: Condens. Matter* **34**, 243002 (2022).
- 21) S. Ikeda, H. Sakai, D. Aoki, Y. Homma, E. Yamamoto, A. Nakamura, Y. Shiokawa, Y. Haga, and Y. Ōnuki, *J. Phys. Soc. Jpn. Suppl.* **75**, 116 (2006).
- 22) H. Harima: submitted to SciPost.
- 23) D. Aoki, A. Nakamura, F. Honda, D. X. Li, Y. Homma, Y. Shimizu, Y. J. Sato, G. Knebel, J.-P. Brison, A. Pourret, D. Braithwaite, G. Lapertot, Q. Niu, M. Vališka, H. Harima, and J. Flouquet, *JPS Conf. Proc.* **30**, 011065 (2020).
- 24) L.P. Cairns, C.R. Stevens, C.D. O'Neill, A. Huxley, *J. Phys.: Condens. Matter* **32**, 415602 (2020).
- 25) Y. Haga, P. Opletal, Y. Tokiwa, E. Yamamoto, Y. Tokunaga, S. Kambe, and H. Sakai, *J. Phys.: Condens. Matter* **34**, 175601 (2022).
- 26) D. Aoki, M. Kimata, Y. J. Sato, G. Knebel, F. Honda, A. Nakamura, D. X. Li, Y. Homma, Y. Shimizu, W. Knafo, D. Braithwaite, M. Vališka, A. Pourret, J.-P. Brison, and J. Flouquet, *J. Phys. Soc. Jpn.* **90** (2021) 074705.
- 27) D. X. Li, A. Nakamura, F. Honda, Y. J. Sato, Y. Homma, Y. Shimizu, J. Ishizuka, Y. Yanase, G. Knebel, J. Flouquet, and D. Aoki, *J. Phys. Soc. Jpn.* **90**, 073703 (2021).
- 28) F. Honda et al. presented at the Japanese Physical Society Annual Meeting (JPS meeting), 12pH3-2 (2021), and Intl' Conf. Low Temperature Physics (LT29), P22-SF3B-31 (2022).
- 29) J. G. Cheng, K. Matsubayashi, S. Nagasaki, A. Hisada, T. Hirayama, M. Hedo, H. Kagi, and Y. Uwatoko, *Rev. Sci. Instrum.* **85**, 093907 (2014).
- 30) L. Havela, M. Diviš, V. Sechovský, A. V. Andreev, F. Honda, G. Oomi, Y. Mérésse, and S. Heathman, *Journal of Alloys and Compd.* **322**, 7 (2001)
- 31) S. Mašková, A.M. Adamska, L. Havela, N.-T.H. Kim-Ngan, J. Przewoźnik, S. Daniš, K. Kothapalli, A.V. Kolomiets, S. Heathman, H. Nakotte, H. Bordallo, *Journal of Alloys and Compd.* **522**, 130 (2012)
- 32) D. Aoki, H. Sakai, P. Opletal, Y. Tokiwa, J. Ishizuka, Y. Yanase, H. Harima, A. Nakamura, D. Li, Y. Homma, Y. Shimizu, G. Knebel, J. Flouquet, and Y. Haga, *J. Phys. Soc. Jpn.* **91**, 083704 (2022).
- 33) J. Ishizuka, S. Sumita, A. Daido, and Y. Yanase, *Phys. Rev. Lett.* **123**, 217001 (2019).

- 34) F. Honda et al., in preparation.
- 35) H. Nowotny, R. Kieffer, and H. Schachner *Monatshefte für Chemie und verwandte Teile anderer Wissenschaften* volume 83, 1243-1252 (1952).
- 36) A. N. Christensen, *Journal of Crystal Growth* **129**, 266-268 (1993).
- 37) V. M. Agoshkov, V. D. Gorbatenkov, S. V. Popova, and L. N. Fomicheva, *Inorg. Mater.*, **17**, 1523-1526 (1981).
- 38) K. Hu, Y. Zhao, Y. Geng, J. Yu, and Y. Gu, *Phys. Lett. A*, **451**, 128401 (2022)
- 39) Q. Niu, G. Knebel, D. Braithwaite, D. Aoki, G. Lapertot, M. Vališka, G. Seyfarth, W. Knafo, T. Helm, J.-P. Brison, J. Flouquet, and A. Pourret, *Phys. Rev. Research* **2**, 033179 (2020).
- 40) T. Helm, M. Kimata, K. Sudo, A. Miyata, J. Stirnat, T. Förster, J. Hornung, M. König, I. Sheikin, A. Pourret, G. Lapertot, D. Aoki, J.-P. Brison, G. Knebel, and J. Wosnitzer, arXiv:2207.08261.
- 41) M. Vališka, W. Knafo, G. Knebel, G. Lapertot, D. Aoki, and D. Braithwaite, *Phys. Rev. B* **104** 214507 (2021), the anomaly at 230 K was reported in the Supplemental Material.
- 42) L. Q. Huston, D. Y. Popov, A. Weiland, M. M. Bordelon, P. F. S. Rosa, R. L. Rowland, II, B. L. Scott, G. Shen, C. Park, E. K. Moss, S. M. Thomas, J. D. Thompson, B. T. Sturtevant, and E. D. Bauer, *Phys. Rev. Mater.* **6**, 114801 (2022).
- 43) V. Sechovsky and L. Havela, *Handbook of Magnetic Materials*, vol. 11, chap. 1, page 1. North-Holland, Amsterdam, 1998.
- 44) F. Wilhelm, J. P. Sanchez, D. Braithwaite, G. Knebel, G. Lapertot, and A. Rogalev: private communication.